Received: 13 February 2024 | Revised: 21 August 2024 | Accepted: 26 August 2024

DOI: 10.1096/fj.202400333RR

RESEARCH ARTICLE

The FASEB Journal

Disruption of HSD17B12 in mouse hepatocytes leads to reduced body weight and defect in the lipid droplet expansion associated with microvesicular steatosis

Hanna Heikelä[1] | **Laura Mairinoja**[1] | **Suvi T. Ruohonen**[1] | **Kalle T. Rytkönen**[1,2] | **Simone de Brot**[3] | **Asta Laiho**[2] | **Satu Koskinen**[2] | **Tomi Suomi**[2] | **Laura L. Elo**[2] | **Leena Strauss**[1] | **Matti Poutanen**[1,4]

[1]Research Centre for Integrative Physiology and Pharmacology and Turku Center for Disease Modeling, Institute of Biomedicine, University of Turku, Turku, Finland

[2]Turku Bioscience Centre, University of Turku and Åbo Akademi University, Turku, Finland

[3]COMPATH, Institute of Animal Pathology, University of Bern, Bern, Switzerland

[4]Department of Internal Medicine and Clinical Nutrition, Centre for Bone and Arthritis Research, Institute of Medicine, The Sahlgrenska Academy, University of Gothenburg, Gothenburg, Sweden

Correspondence
Matti Poutanen, Research Centre for Integrative Physiology and Pharmacology, Institute of Biomedicine, University of Turku, Kiinamyllynkatu 10, FI-20520 Turku, Finland.
Email: matti.poutanen@utu.fi

Funding information
Sigrid Juséliuksen Säätiö (Sigrid Jusélius Stiftelse); UTU | Institute of Biomedicine, University of Turku (Biolääketieteen laitos); Jalmari ja Rauha Ahokkaan Säätiö (Jalmari and Rauha Ahokas Foundation)

Abstract

The function of hydroxysteroid dehydrogenase 12 (HSD17B12) in lipid metabolism is poorly understood. To study this further, we created mice with hepatocyte-specific knockout of HSD17B12 (LiB12cKO). From 2 months on, these mice showed significant fat accumulation in their liver. As they aged, they also had a reduced whole-body fat percentage. Interestingly, the liver fat accumulation did not result in the typical formation of large lipid droplets (LD); instead, small droplets were more prevalent. Thus, LiB12KO liver did not show increased macrovesicular steatosis with the increasing fat content, while microvesicular steatosis was the predominant feature in the liver. This indicates a failure in the LD expansion. This was associated with liver damage, presumably due to lipotoxicity. Notably, the lipidomics data did not support an essential role of HSD17B12 in

Abbreviations: 20-HETE, 20-hydroxyeicosatetraenoic acid; AA, arachidonic acid; ALP, alkaline phosphatase; ALT, alanine aminotransferase; AUC, area under the curve; BSA, bovine serum albumin; CE, cholesterol esters; CER, ceramide; Cidec, cell death-inducing DFFA-like effector C; CTRL, control; Cyp, cytochrome P450; DAG, diacylglycerols; DCER, dihydroceramide; EET, epoxyeicosatrienoic acid; FA, fatty acid; FC, fold change; FFA, free fatty acids; Fitm2, fat storage inducing transmembrane protein 2; Flot1, flotillin 1; GTT, glucose tolerance test; H&E, hematoxylin and eosin; HCER, hexosylceramide; Hilpda, hypoxia inducible lipid droplet associated; HSD17B, hydroxysteroid 17-beta-dehydrogenase; HSD17B12, hydroxysteroid 17-beta dehydrogenase type 12; ITT, insulin tolerance test; KO, knockout; LCER, lactosylceramide; LD, lipid droplet; LiB12cKO, hepatocyte-specific knockout of HSD17B12; LPC, lysophosphatidylcholine; LPE, lysophosphatidylethanolamine; Mrpl19, Mitochondrial ribosomal protein L19; NAFLD, nonalcoholic fatty liver disease; NASH, nonalcoholic steatohepatitis; PC, phosphatidylcholine; PE, phosphatidylethanolamine; Plin, perilipin; Pnpla3, patatin-like phospholipase domain-containing protein 3; SD, standard deviation; SM, sphingomyelin; *Smpd3*, sphingomyelin phosphodiesterase 3; TAG, triacylglycerol; TUNEL, terminal deoxynucleotidyl transferase dUTP nick end labeling; VLCFA, very long-chain fatty acid.

fatty acid (FA) elongation. However, we did observe a decrease in the quantity of specific lipid species that contain FAs with carbon chain lengths of 18 and 20 atoms, including oleic acid. Of these, phosphatidylcholine and phosphatidylethanolamine have been shown to play a key role in LD formation, and a limited amount of these lipids could be part of the mechanism leading to the dysfunction in LD expansion. The increase in the *Cidec* expression further supported the deficiency in LD expansion in the LiB12cKO liver. This protein is crucial for the fusion and growth of LDs, along with the downregulation of several members of the major urinary protein family of proteins, which have recently been shown to be altered during endoplasmic reticulum stress.

KEYWORDS

17-hydroxysteroid dehydrogenases, computer assisted image analysis, lipid droplets, liver steatosis, nonalcoholic fatty liver disease

1 | INTRODUCTION

The liver synthesizes fatty acids (FA) from non-lipid sources and builds important lipoproteins. In a healthy state, lipids are not stored in the liver for long periods. Instead, the extra energy from the diet is packed in lipid droplets (LDs) and lipoprotein particles in the liver, destined for subsequent transport to adipose tissue for long-term storage. However, when these processes are disturbed, LDs accumulate in hepatocytes resulting in hepatic steatosis. Nonalcoholic fatty liver disease (NAFLD) and its more severe form of nonalcoholic steatohepatitis (NASH) are growing health problems in developed countries.[1] Steatohepatitis is heavily associated with type 2 diabetes and obesity, and its prevalence continues to rise in Western countries as the incidences of metabolic diseases increase.[2] Moreover, NASH may progress to liver fibrosis and even to cirrhosis.[3] Furthermore, it increases the risk of hepatocellular cancer. Despite the high association with obesity, NAFLD does occur in lean individuals as well and there is strong evidence, that NAFLD is associated with an increased risk of cardiovascular diseases, independently of traditional cardiovascular risk factors, such as obesity or diabetes.[4]

Hydroxysteroid 17beta-dehydrogenases (HSD17B) enzymes belong to the family of short-chain dehydrogenases/reductases.[5] According to the name of the enzymes, some of them are involved in steroid metabolism by catalyzing the interconversion between 17-ketosteroids and 17-hydroxysteroids.[6] However, some of the HSD17B-enzymes are involved in cholesterol or retinol metabolism, FA oxidation, or other pathways of lipid metabolism.[6] HSD17B12 was first characterized in vitro as 3-ketoacyl coenzyme A reductase in 2003.[7] Using genetically modified mice, we have previously reported that HSD17B12 is essential for early embryonic development, with a decreased proliferation capacity in the knockout (KO) blastocysts,[8] and mice with a hypomorphic *HSD17B12* allele showed reduced capacity for prostaglandin synthesis in the ovary that was associated with defect in the regulation of meiosis of the oocytes.[9] Interestingly, widespread deletion of the HSD17B12 gene in adult mouse tissues by crossbreeding the *Hsd17b12* floxed mouse strain with inducible ROSA26-Cre-ERT mice leads to drastic weight loss, malaise, and eventually death in about a week. In addition, these mice presented with microvesicular liver steatosis.[10] These results have shown a vital role for HSD17B12 in multiple physiological processes.

To further study the metabolic role of HSD17B12, in the present study, we have generated a liver-specific HSD17B12KO mouse model by crossbreeding the mouse strain with floxed *Hsd17b12* gene with mice expressing the *Cre*-recombinase under the albumin promoter. The mice presented with reduced body adiposity associated with the accumulation of triacylglycerols (TAG), diacylglycerols (DAG), and cholesterol ester (CE) in the hepatocytes as a form of microvesicular steatosis. These metabolic defects were accompanied by a deficiency in the LD biogenesis in the liver.

2 | MATERIALS AND METHODS

2.1 | Animals

All animal work was conducted at the Central Animal Laboratory at the University of Turku, Finland, under the animal license numbers 10605/04.10.07/2016 and 41729/2019, granted by the Animal Experiment Board in Finland. Animal handling was carried out in accordance

with the institutional animal care policies that fully meet the requirements as defined in the National Institutes of Health (Bethesda, MD, USA) guidelines on animal experimentation.

Animals were housed in individually ventilated cages (IVC, Techniplast, Buguggiate, Italy) with approximately 70 air changes per hour. Constant temperature (21 ± 3°C) and humidity (55 ± 15%) were maintained together with a 12 h light–dark cycle, with a light change at 7 am and 7 pm. Autoclaved aspen chips were used as bedding (Tapvei Ltd, Harjumaa, Estonia). Soy-free pellets (RM3, Special Diets Services, Essex, UK) and water were available *ad libitum*. The animals were individually identified by ear markings and housed with littermates, 1–6 mice per cage. Animals were sacrificed using CO_2 asphyxiation and cervical dislocation at the ages of 2, 6, or 8 months.

2.2 | Generation of conditional KO mice

A mouse strain with floxed Hsd17b12 gene[10] was crossbred with mice expressing the Cre-recombinase under the albumin promoter[11] to generate a liver-specific KO mouse strain LiB12cKO. The albumin promoter directs the Cre recombination in hepatocytes, from the time when hepatocytes begin to replace hematopoietic cells in the fetal liver on embryonic day 10[12,13] and continues until the postnatal age of 6 weeks.[14] Schematic representations of the targeted, floxed, and deleted alleles, as well as the breeding systems and cohorts, are shown in Figure S1. The pups were earmarked and genotyped with PCR at the age of 14 days, and the genotypes used for the experiments included HSD17B12$^{lox/lox}$; Alb-Cre$^{Cre/WT}$ (KO), and HSD17B12$^{lox/lox}$; Alb-Cre$^{WT/WT}$ (control) animals. The primer pairs used for genotyping are listed in Table 1.

2.3 | Histological analysis

Tissue samples were fixed in 10% formalin for 24–48 h and dehydrated in 70% ethanol. Fixed tissues were embedded in paraffin. And 4 μm thick sections were cut from the left lateral liver lobe. Two to three sections per animal were stained with hematoxylin–eosin (H&E) staining following standard procedures. The images were visually analyzed for pathological changes. Hepatocellular swelling was interpreted as hypertrophy and was characterized by variable cytoplasmic eosinophilia (indicative for an increase in the number of organelles) and rarification due to hydropic change or glycogen accumulation, or both.

TABLE 1 Primers used for genotyping PCR and qRT-PCR assays.

Target		Sequence (5′–3′)	Amplicon size (bp)	Annealing T (C)
Genotyping PCR				
Hsd17b12 (Lox P)	For	TTAGGCTTTACTAGCATATAGC	206 (wt)	60.0
	Rev	TATAAGGAAACGGAAGCTCA	400 (loxP)	
Alb-Cre wt	For	TGCAAACATCACATGCACAC	351 (wt)	57.0
	Rev	TTGGCCCCTTACCATAACTG		
Alb-Cre mut	For	GAAGCAGAAGCTTAGGAAGATGG	390 (mut)	60.0
	Rev	TTGGCCCCTTACCATAACTG		
qRT-PCR				
Mrp19	For	GGACAGAGTCTTGATGATCTC	195	60.0
	Rev	CTGAAGGTCAAAGGGAATGTG		
Hsd17b12	For	GCAGTTGTTACAGGTGGCAC	250	59.6
	Rev	TGCCCACGTTGTTCACTAAA		
Cyp2c29	For	TCACAACTGTGTCAGTAAGGAGG	226	61.8
	Rev	GTGAACACAGGGCCATAAGC		
Cyp2c50	For	ATGAGGCAGTGAAGGAAGCT	205	61.8
	Rev	TCCTCTTGAACACGGTCCTC		
Cyp4a10	For	TTCCCTGATGGACGCTCTTTA	116	59.0
	Rev	GCAAACCTGGAAGGGTCAAAC		
Cyp4a14	For	CTGGGGAGATCAGATCCAAA	174	59.0
	Rev	GACAGAGTCCGCCATGATTT		

Abbreviations: bp, base pairs; For, forward; Rev, reverse.

For each mouse, the severity of these changes was graded subjectively with a range from 0 to 3, depending on the prevalence of hypertrophy.

Immunohistochemical staining for Ki-67 was performed on 4 μm thick sections using Labvision™ autostainer (Thermo Fisher Scientific). Antigen retrieval was performed in citrate buffer (pH 6) (Genemed Biotechnologies, Torrance, CA, USA) using a pressure cooker for 20 min and sections were washed with 0.05 M Tris–HCl (Reagena, Toivala, Finland) with 0.05% Tween 20 added. The primary antibody (Ki-67 Monoclonal Antibody, SolA15, eBioscience™, Thermo Fisher Scientific, Waltham, MA, USA) was diluted 1:2000 (0.25 ug/mL), applied for the sections, and the sections were incubated at room temperature for 60 min. The sections were then further incubated with the secondary antibody (Rat on mouse HRP-polymer, Biocare Medical, Pacheco, CA, USA), at room temperature for 30 min and counterstained with Mayer's hematoxylin (Histolab Products AB, Västra Frölunda, Sweden) before mounting with Pertex mounting medium (Histolab Products AB).

Terminal deoxynucleotidyl transferase dUTP nick end labeling (TUNEL) was performed on 4 μm thick tissue sections. Antigen retrieval was performed in citrate buffer in a microwave oven. The endogenous peroxidase activity was then blocked by applying 3% H_2O_2. TUNEL reaction mixture containing TdT and biotin−16-dUTP (Roche Diagnostics GmbH) was applied to the sections and incubated at 37°C for 1 h. Thereafter, the reaction was stopped by adding 300 mM NaCl, treated with 3% bovine serum albumin (BSA), and incubated in ExtrAvidine (Sigma-Aldrich, diluted 1:500 in 1% BSA) for 30 min at 37°C, followed by staining with 3,3′ diaminobenzidine (Dako Liquid DAB+ Substrate Chromogen System; Dako North America, Carpinteria, CA, USA). Finally, the sections were counterstained with Mayer's hematoxylin, dehydrated, and mounted. The slides were scanned with a 3DHISTECH Pannoramic 250 Flash III slide scanner (RRID:SCR_022184) (3DHISTECH Ltd., Budapest, Hungary) and visualized using CaseViewer (RRID:SCR_017654) software version 2.3. (3DHISTECH Ltd).

2.4 | Image analysis and quantification of apoptosis, proliferation, and steatosis

Hepatic steatosis was quantified from digitized whole slide images (WSIs) of H&E-stained sections with a computerized, deep learning-based, method created in the Aiforia (RRID:SCR_022739) Create (version 5.3, Aiforia Technologies, Helsinki, Finland). For analysis, one section per animal was examined. The model detects liver parenchyma, including normal hepatocytes, macrovesicular hepatocytes, and microvesicular hepatocytes, and excludes tissue artifacts, blood vessels, and other features that do not belong to the liver parenchyma (Figure S2). The model was trained so that inside parenchyma, the tissue was considered to contain macrovesicular steatosis if the single LDs were bigger than the average size of the nucleus and microvesicular steatosis if the LDs were smaller than the average size of the nucleus.[15]

For TUNEL and Ki-67 analyses, the QuPath (RRID:SCR_018257) open-source software platform (version 0.2.0) was used.[16] The digitized WSIs were converted to mrxl image format, to be used with QuPath. Apoptosis and cell proliferation were quantitated using the feature of positive cell detection, where parameters were set to optimally detect both the Hematoxylin-stained nuclei and the TUNEL and Ki-67 positive cells (Figure S2). The proportion of the positive cells of all cells was then calculated from the whole area of four tissue sections on each slide.

2.5 | GTT and ITT

Glucose tolerance test (GTT) and insulin tolerance test (ITT) were performed for 6-month-old mice, GTT for both males and females and ITT only for males. The mice were fasted for 6 h before GTT and 1 h before ITT. Fasting glucose concentration was measured with FreeStyle Lite blood sugar monitoring system (Abbott Diabetes Care Inc., Alameda, CA, USA). A glucose dose of 2 g/kg (GTT) or 0.75 U/kg of insulin (ITT) was given via intraperitoneal injection (time 0), and blood sugar measurements were repeated at 20-, 40-, 60- and 90-min timepoints. The results were analyzed with two-way ANOVA.

2.6 | Measurement of biomarkers for liver dysfunction and systemic inflammation

At the age of 10 weeks, 100 μL of blood were collected via saphenous vein from 8 control (CTRL) and 8 LiB12cKO males and 10 CTRL and 10 LiB12cKO females in lithium-heparin tubes (Becton, Dickinson and Company, Franklin Lakes, NJ, USA). The samples were then analyzed using VetScan® Mammalian Liver Profile reagent rotor (Abaxis, Inc., Union City, CA, USA), which measured the following parameters: total bilirubin, blood urea nitrogen, alkaline phosphatase (ALP), alanine aminotransferase (ALT), gamma-glutamyl transferase, bile acids, albumin, and total cholesterol. The analysis was run by using the

VetScan Chemistry Analyzer (Abaxis, Inc. Union City, CA, USA) in the Central Animal Laboratory at the University of Turku. Interleukin 6 (IL-6) levels in the serum were measured in 2-, 6-, and 8-month-old males. Blood was collected via heart puncture and let to coagulate at +4°C overnight before serum was separated by centrifugation at 3000 × *g* for 15 min. Measurement was carried out using Quantikine™ ELISA IL-6 Immunoassay-kit (Bio-Techne, Minneapolis, Mn, USA) according to the manufacturer's instructions. Optical density was determined at 450 and 540 nm using Ensight platereader (PerkinElmer Inc., Waltham, Ma, USA).

2.7 | Body weight and composition

Mouse body weight was recorded at the ages of 2, 6, and 8 months. Body composition was measured with the EchoMRI-700™ device (Echo Medical Systems, Houston, TX, USA) in live animals at the ages of 6 and 8 months.

2.8 | RNA extraction, RT-qPCR analysis, and RNA sequencing

Total RNA was extracted from frozen liver tissues of 2-month-old male mice using TRIsure™ (Bioline, London, UK) and DNase-treated using a DNase I kit (Sigma-Aldrich, Saint Louis, MO, USA). RNA was reverse transcribed using SensiFAST™ cDNA Synthesis kit (Bioline) and RT-qPCR analysis was performed using Sybr Green kit (Thermo Fisher Scientific, Waltham, MA, USA) and analyzed using Bio-Rad CFX96 Real-Time PCR Detection System (RRID:SCR_018064) (Bio-Rad, Hercules, CA, USA) combined with CFX Manager (RRID:SCR_017251) software (Bio-Rad). The primers used in RT-qPCR are listed in Table 1.

RNA sequencing of total RNA was performed using an Illumina NovaSeq 6000 Sequencing System (RRID:SCR_016387) (Illumina, San Diego, CA, USA) at Novogene (Cambridge, UK). The sequencing length was 150 base pairs from both ends and the sequencing depth was 20 million reads per sample. The read quality was checked with FastQC (v.0.11.14) (RRID:SCR_014583),[17] and the reads were aligned to mm10 and assigned to genes with Rsubread (RRID:SCR_016945) (v.2.0.0).[18] edgeR (RRID:SCR_012802) (v.3.28.0)[19] was used for normalization to counts per million (CPM) and ROTS (v.1.14.0)[20] for the analysis of differential expression. Differentially expressed genes with FDR <0.05 and absolute fold change (FC) >2.0 were selected for functional enrichment analysis using Metascape (RRID:SCR_016620) (metascape.org) with default functional categories from GO Biological Processes (GO), KEGG (K) and Reactome (R). Additional enrichment analysis was done using the DisGeNET (RRID:SCR_006178) database. The heatmap visualization of selected gene sets was conducted with RPKM (reads per kilobase per million mapped reads) using pheatmap_1.0.12 in R Project for Statistical Computing (RRID:SCR_001905) 3.5. Hierarchical clustering was performed using Euclidean distance and *Ward's* minimum variance method. The sequencing results are available at Gene Expression Omnibus (RRID:SCR_005012) repository under the series accession number GSE255345.

2.9 | Liver lipidomics

Liver samples were collected from 10 CTRL and 10 LiB12cKO male mice at the age of 2 months. Lipids were extracted using the liquid–liquid extraction method, using ethyl acetate and methanol as the extraction solvents. Frozen liver samples (20 mg) were transferred to precellys ceramic tubes, and 1 mL of water was added to homogenize the tissues using a tissue homogenizer at 5500 rpm for three cycles. The homogenized mixture was then transferred to glass tubes, and 1 mL of methanol (VWR International, Helsinki, Finland) along with 100 µL of a labeled internal standard mixture (prepared according to the instructions in the Sciex Lipidyzer manual) was added. An internal standard kit containing 50 labeled internal standards across 13 lipids classes was purchased from AB Sciex (Washington, D.C., USA). The mixture was allowed to equilibrate with the samples, 3.5 mL of ethyl acetate (VWR International) was added, and the tubes were placed on a rotator shaker for 15 min, rotating at a speed of 30 rpm. This was followed by centrifugation at 3000 rpm for 10 min. After centrifugation, the upper layer of ethyl acetate was collected and dried under nitrogen. Dried samples were reconstituted with 250 µL of dichloromethane:methanol (50:50), containing 10 millimolar ammonium acetate for injection. Ammonium acetate was obtained from Sigma-Aldrich (Helsinki, Finland). Lipid separation and quantification were done using the SCIEX LIPIDYZER platform utilizing the SCIEX 5500 QTRAP 5500 Mass Spectrometer (RRID:SCR_020517) (Sciex, Washington, D.C., USA) with SelexION (Differential ion mobility) DMS technology. The analysis involved direct infusion of 50 µL of extracted samples with the mobile phase at a flow rate of 70 µL/min. Two acquisition methods, with and without SelexION® technology, were used, covering 13 lipid classes using a flow injection analysis. The lipid molecular species were measured using the MRM strategy in both positive and negative polarities. Positive ion mode was used for the detection of the lipid classes of sphingomyelins (SM), DAG, CE, ceramides (CER), dihydroceramides (DCER),

TAG, and negative ion mode was used for the detection of the lipid classes of lysophosphatidylethanolamine (LPE), lysophosphatidylcholine (LPC), phosphatidylcholines (PC), phosphatidylethanolamine (PE), and free fatty acids (FFA). Lipidomics Workflow Manager software was used for sample acquisition and automated data processing, signal detection, and lipids species concentration calculations. Lipidomics analyses were performed in FIMM, Helsinki, Finland.

2.10 | Statistics

GraphPad Prism (RRID:SCR_002798) 8.1.2 software (GraphPad Software, La Jolla, CA, USA) was used to carry out statistical analyses. Outliers were identified using the ROUT method in Prism with a coefficient of $Q=1\%$. Statistical tests were chosen depending on the results of the Shapiro–Wilk tests of data normality. An unpaired *t*-test or nonparametric Mann–Whitney test was used to determine the statistical significance between two groups at a single timepoint and two-way ANOVA for multiple time points unless otherwise indicated. The area under the curve (AUC) (baseline at 0 min) was used to analyze GTT and ITT results. The threshold for statistical significance was set at $p<0.05$ and the results were expressed as mean ± standard deviation (SD) unless otherwise indicated.

3 | RESULTS

3.1 | Disrupting the *HSD17B12* gene in hepatocytes decreases body mass and body fat content

To study the role of HSD17B12 in the liver in vivo, we generated a mouse model with *Hsd17b12* deficiency in the hepatocytes. For this purpose, we crossed mice carrying loxP-sequences around the exon 2 of the *Hsd17b12* gene with mice expressing the *Cre*-recombinase activity under the albumin promoter, initiated during fetal development. As a result, the open reading frame of HSD17B12 is disrupted, and additionally, the expression of the mutated allele was shown to be decreased compared with the mice without the *Cre*-expression or with mice expressing the wild-type HSD17B12 (Figure S1C). All genotypes were born in the expected Mendelian ratio and were viable until late adulthood (data not shown). The LiB12cKO mice did not differ from the CTRL mice in terms of body weight or body composition at the age of 2 months. However, at the age of six and 8 months, the LiB12cKO had significantly reduced body weight compared with the age-matched CTRL mice (Figure 1A). Accordingly, body composition measurements showed significantly lower relative body fat content in 6-month-old LiB12cKO females compared with CTRL females (FC = −1.57, $p=.010$), but in 6-month-old males, the difference was not significant (CTRL mean = 12.4%, KO mean = 10.5%). At the age of 8 months, both male and female LiB12cKO mice had significantly lower body fat percentage than the CTRL mice (males, FC = −1.34, $p=.028$; females, FC = −1.63, $p\leq.001$) (Figure 1B). There was no difference in the lean mass in female mice at 6 or 8 months of age, or in the 8-month-old males, while at the age of 6 months, the male LiB12cKO mice showed also slightly lower total lean mass (Figure 1C) than the CTRL males (FC = −1.07, $p=.023$).

The male LiB12cKO mice appeared to be more tolerant to glucose injection than the CTRL mice, by showing significantly lower total glucose levels in all data points after the glucose administration (Figure 1D), resulting in a 42% smaller AUC value in the LiB12cKO mice compared with CTRLs (AUC for CTRL = 1598 and LiB12cKO =922.4). A similar trend was also observed in the females (AUC for CTRL = 1067 and LiB12cKO =978). We also tested the tolerance to insulin to see whether the difference observed in the glucose tolerance was due to insulin sensitivity, but there was no significant difference between the study groups in either sex (AUC for males: CTRL = 630.8 and LiB12cKO =563 and females: CTRL = 591.4 and LiB12cKO = 482.8) (Figure 1E). Together these results indicate that *Hsd17b12* disruption in hepatocytes leads to decreased body weight in mice, as a result of reduced adiposity during aging, accompanied by improved glucose tolerance in males.

3.2 | Disrupting the *HSD17B12* gene in hepatocytes leads to increased steatosis accompanied by suppressed LD biogenesis

Both male and female LiB12cKO mice showed significantly larger livers than the CTRL mice in all age groups studied (Figure 1F). This difference was notable already in 2-month-old mice (males, FC = 2.11, $p\leq.001$; females, FC = 1.57, $p=.001$). In 6-month-old mice, the difference was even greater (males, FC = 2.31, $p\leq.001$; females, FC = 1.65, $p=.002$), and at the age of 8 months, the difference was still persistent (males, FC = 1.51, $p=.001$; females, FC = 1.64, $p\leq.001$). In addition, the livers of the 2-month-old LiB12cKO mice were pale, a feature that often indicates the appearance of fatty liver (Figure 1G). Accordingly, the H&E-stained sections of the LiB12cKO livers showed an increased number of empty vacuoles, considered to represent LDs already at 2 months of age, and the difference was constant over the study period

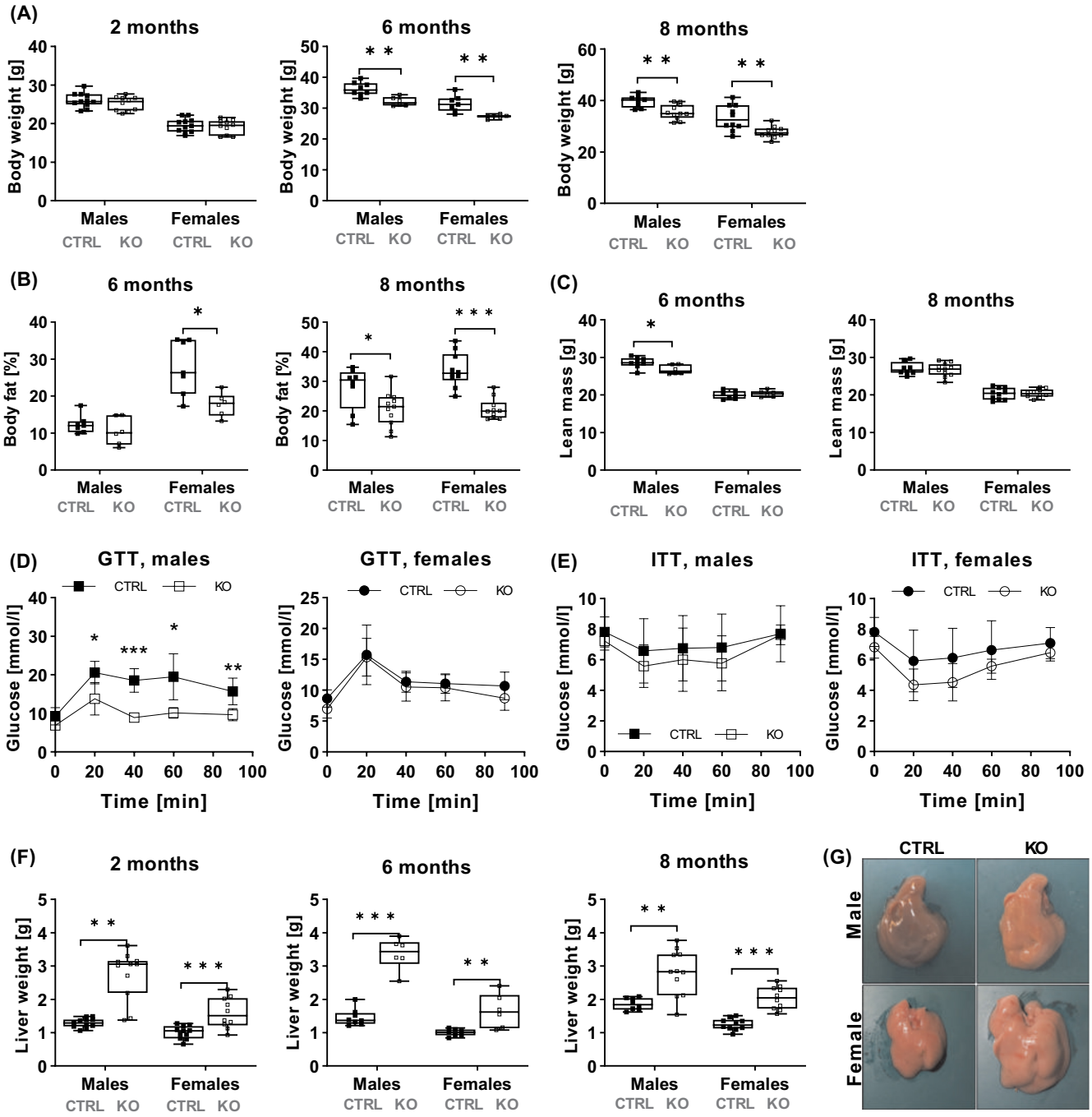

FIGURE 1 The LiB12cKO (KO) mice have lower body fat than control (CTRL) mice. (A) Body weight of 2-month-old (males CTRL, $n=11$; males KO, $n=11$; females CTRL, $n=10$; females KO, $n=10$) 6-month-old (males CTRL, $n=8$; males KO, $n=6$; females CTRL, $n=7$; females KO, $n=6$; males fold change (FC) $=-1.13$, $p=.002$; females FC $=-1.15$, $p=.004$) and 8-month-old (males CTRL, $n=8$; males KO, $n=11$; females CTRL, $n=10$; females KO, $n=10$; males FC $=-1.12$, $p=.003$; females FC $=-1.20$, $p=.005$) mice, (B) body fat percentage and (C) body lean mass of 6- and 8-month-old mice, (D) glucose tolerance test (GTT) results as well as (E) insulin tolerance test (ITT) results of 6-month-old mice. (F) Liver weights of 2- (males CTRL, $n=11$; males KO, $n=11$; females CTRL, $n=10$; females KO, $n=10$) 6- (males CTRL, $n=8$; males KO, $n=6$; females CTRL, $n=7$; females KO, $n=6$) and 8-month-old (males CTRL, $n=8$; males KO, $n=11$; females CTRL, $n=10$; females KO, $n=10$) mice. (G) Macroscopic images of livers of 2-month-old CTRL and LiB12cKO (KO) mice. KO livers present with diffuse pallor and hepatomegaly, consistent with hepatic lipidosis. *T*-test for comparing CTRL and KO mice, except for GTT and ITT, two-way ANOVA. $^{*}p < 0.05$, $^{**}p < 0.01$, $^{***}p < 0.001$.

(Figure 2A). Micro- and macrovesicular steatosis was quantified by a recently developed deep learning-based model for quantifying hepatic steatosis (Figure 2B), and markedly higher areas of microvesicular steatosis were identified in LiB12cKO male liver already at the age of 2 months compared with CTRLs. This difference between

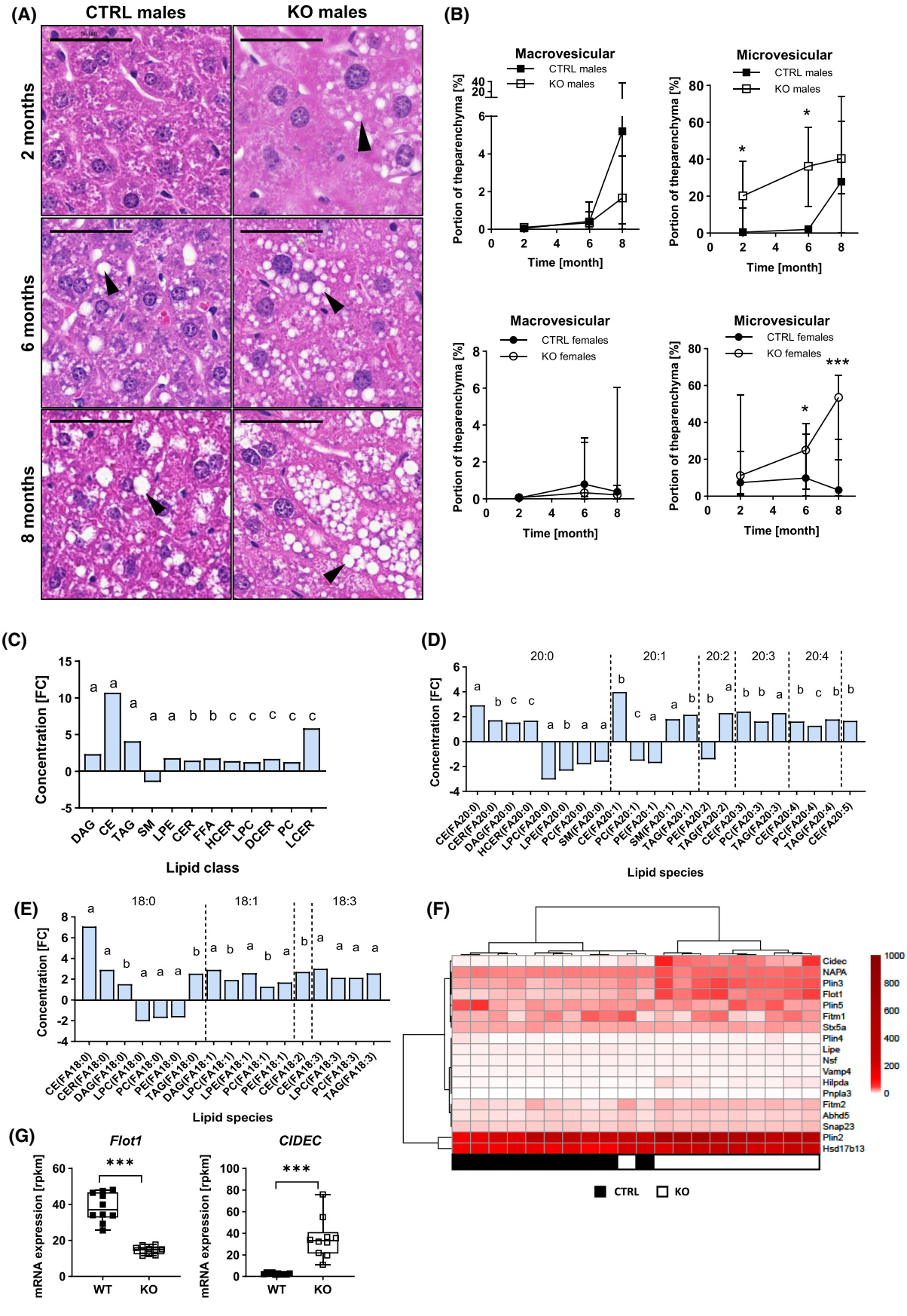

FIGURE 2 LiB12cKO mice develop fatty livers. (A) Hematoxylin–eosin-stained liver tissue of 2- and 6- and 8-month-old control (CTRL) and LiB12cKO (KO) male mice showing lipid droplets (LD) (arrowheads). Scale bar 50 μm. (B) Quantification of macrovesicular and microvesicular steatosis areas by image analysis (median with upper and lower 95% confidence limits). (C) Lipid class concentration fold changes (FCs) between LiB12cKO and CTRL mice. (D) Significantly changed lipid species containing a fatty acid (FA) with chain length of 20 carbon atoms and (E) 18 carbon atoms. Adjusted *p*-values (a) <.001, (b) ≤.01 (c) <.05. (F) mRNA expression of lipid droplet (LD)-associated genes in the liver LiB12cKO and CTRL mice, reads per kilobase per million mapped reads (RPKM). (G) Gene expression of cell death-inducing DFFA-like effector C (*CIDEC*) and flotillin 1 (*Flot1*), chosen from LD-associated genes. *$p < 0.05$, ***$p < 0.001$; and a: $p < 0.001$, b: $p < 0.01$, c: $p < 0.05$.

the genotypes remained throughout the 8-month-long study period (FC = 7.60, $p = .0015$ at 2 months of age; FC = 18.74, $p = .0012$, at 6 months of age). The dynamics were different in the females, as there was no difference between the genotypes in the 2- and 6-month-old mice, but at 8-month-old LiB12cKO females, the areas with microvesicular steatosis were highly increased (FC = 4.25, $p = .0007$). Furthermore, the formation of macrovesicular steatosis was hindered in LiB12cKO males, resulting in an increased ratio of microsteatosis/macrosteatosis in the LiB12cKO mice.

At the age of 2 months, the LiB12cKO male mice showed increased concentration of most lipid classes, with the highest differences in CE (FC = 10.72, $p \leq .001$), LCER (FC = 5.86, $p = .031$) and TAG (FC = 4.09, $p \leq .001$). TAG and CE are the most common neutral lipids stored in the LDs, thus, likely making them the major lipid classes resulting in the increased microsteatosis phenotype in the LiB12cKO livers. However, significant upregulation was also observed in the concentrations of DAG (FC = 2.33, $p \leq .001$), LPE (FC = 1.79, $p \leq .001$), FFA (FC = 1.77, $p = .014$), DCER (FC = 1.68, $p = .03$), CER (FC = 1.45, $p = .01$), HCER (FC = 1.39, $p = .03$), LPC (FC = 1.26, $p = .03$) and PC (FC = 1.26, $p = .03$). Interestingly, only SM class showed decreased concentrations (FC = −1.45, $p \leq .001$) in the LiB12cKO livers (Figure 2C). Furthermore, principal component analysis separated the CTRL and LiB12cKO mice into different clusters based on the composition of lipid species (Figure S3). Interestingly, the expression of *Smpd3*, which codes for SM phosphodiesterase 3, was 8.5 times higher in the LiB12cKO mice liver compared with the CTRL group livers (data not shown). This enzyme hydrolyzes SM to form CER and PC, and its increased expression is in line with reduced SM concentration in the KO livers. Surprisingly, the most abundant LD monolayer components were only moderately increased (PC) or not changed (PE) in concentration, even though the number of visible microsteatotic LDs was higher in the LiB12cKO livers.

The HSD17B12 enzyme has been suggested to be involved in the elongation of FAs, especially in the conversion of 18-carbon FAs into 20-carbon FAs. However, no reduction was observed in the levels of arachidonic acid (AA) (20:4), eicosapentaenoic acid (20:5), or any other FAs with a chain length of 20 carbon atoms (Figure 2D). Similarly, we did not observe any specific accumulation of 18:2 or 18:3 carbon chain FAs, which are precursors for the formation of AA and eicosapentaenoic acid (Figure 2E). There was no major change in the concentration of lipid species containing the FA 20:4. Interestingly, there was a decrease in the saturated FAs with the chain length of 18 and 20 carbon atoms incorporated in the phospholipids, including LPC, LPE, PC, PE, and SM. Overall, the lipidomic analysis does not support the role of HSD17B12 as a rate-limiting step in the elongation of AA or other FAs with similar chain lengths.

The RNA sequencing of the livers showed a clustering of the samples based on the genotype (Figure S4). The differentially expressed genes showed that *Hsd17b12* disruption in the hepatocytes affected the expression of 1112 genes in the liver. The 20 most upregulated and the 20 most downregulated genes are presented in Table S1. Several LD-associated genes were among the upregulated transcripts in the LiB12cKO animals (Figure 2F). The highest FC was observed for cell death-inducing DFFA-like effector C (*Cidec*) (10.42, fdr ≤0.001), others included patatin-like phospholipase domain-containing protein 3 (*Pnpla3*) (FC = 2.85, fdr ≤0.001), flotillin 1 (*Flot1*) (2.54, fdr = 0.00022), hypoxia inducible LD-associated (*Hilpda*) (FC = 2.11, fdr≤0.001), perilipin 2 (*Plin2*) (FC = 1.91, fdr = 0.0013), *Plin3* (FC = 1.78, fdr = 0.0013) and fat storage inducing transmembrane protein 2 (*Fitm2*) (FC = 1,74, fdr = 0.0027). The difference in the mRNA levels of the two most interesting of these, *CIDEC* and *Flot1* between the CTRL and LiB12cKO mice, are illustrated in Figure 2G. The other interesting feature of the transcriptomic data is the large number of major urinary proteins being heavily downregulated in the liver of the LiB12cKO mice, suggesting the presence of endoplasmic reticulum stress in the liver as one of the immediate responses to HSD17B12 deficiency. The data above further suggests that LD formation was affected by the *Hsd17b12* disruption in the hepatocytes.

3.3 | The hepatocyte-specific deletion of the HSD17B12 gene causes liver damage

The levels of the widely used serum markers for liver damage, ALT, and ALP, were increased in both male and female mice at the age of 2 months (Table 2). Liver damage was indicated also by the quantification of apoptotic

cells by TUNEL staining, showing a significantly higher percentage of apoptotic hepatocytes in LiB12cKO males compared with CTRL males at the ages of 6 and 8 months (FC = 15.7, $p = .008$ and FC = 44.4, $p = .022$) (Figure 3A,B), while in 2-month-old females, such difference was not observed. The results also showed a significantly higher percentage of hepatocytes positive for immunohistochemical staining for Ki-67 in males in all age groups (2 months: FC = 2.64, $p = .006$; 6 months: FC = 2.81, $p \leq .001$; 8 months: FC = 2.89, $p \leq .001$) and in 2-month-old females (FC = 1.86, $p = .008$), indicating an increased hepatocyte proliferation at the age of 2 months onwards (Figure 3C,D). This suggests the activation of the regenerative pathway in response to hepatocyte damage in the LiB12cKO mice.

Visual analysis of the H&E-stained liver sections revealed increased hepatocellular hypertrophy in the LiB12cKO mice (Figure 3E,F). Hypertrophy was characterized as cellular swelling with cytoplasmic eosinophilia, vacuolation, and rarification, and it was present in varying degrees in all 2–8-month-old male KO mice ($n = 6$–10), while 0–25% of the CTRL mice at these age groups presented with hypertrophic hepatocytes ($n = 8$–11). In females, hypertrophy was present in 83–100% of all age groups of the KO mice ($n = 10$), compared with 20–43% of the CTRL mice ($n = 7$–11). Interestingly, signs of a relevant hepatic inflammation were not observed in any age group of either sex. Moreover, to assess the presence or absence of systemic inflammation, we measured the concentration of a well-known inflammation marker, Interleukin 6, in serum samples of male mice at the age of 2, 6, and 8 months. These results did not show significant differences between the genotypes in any age group (Figure 3G).

The appearance of hepatocyte damage is also shown by functional enrichment analysis of the RNA sequencing data carried out with DisGeNET Gene Disease Database (Figure 4A) and Metascape (Figure 4B) pathway databases, with the enriched pathway terms including liver injury, liver toxicity, and response to toxic substance. These findings provide evidence for the presence of lipid toxicity in the liver of LiB12cKO mice. The accumulation of toxic compounds in the LiB12cKO liver was also suggested in Metascape analysis (Figure 4B), and among the others, the data showed an alteration in the development of fibrosis-related events (response to wounding, the supramolecular fiber organization, extracellular structure-organization, and regulation of cell adhesion).

In line with the liver histology and lipid analyses, the RNA sequencing data showed a strong association between HSD17B12 KO and fatty liver disease, hyperlipidemia, and nonalcoholic fatty liver disease (Figure 4A). The analysis also indicated that the metabolic process of monocarboxylic acid was one of the pathways upregulated in the LiB12cKO mice. Also, several genes involved in eicosanoid metabolism, such as *Cyp4a10 and Cyp4a14*, which are thought to be involved in the synthesis of 20-hydroxyeicosatetraenoic acid (20-HETE), were upregulated in the KO livers in 2-month- (FC = 4.87, $p \leq .001$ and FC = 29.4, $p \leq .001$, respectively) and 6-month-old males (FC = 4.0, $p = .004$ and FC = 29.3, $p \leq .001$, respectively) (Figure 4C,D). Simultaneously, several genes that are thought to participate in the production of epoxyeicosatrienoic acid (EET), such as *Cyp2c29, Cyp2c37, Cyp2c50*, and *Cyp2c54* were downregulated in the KO livers (Figure 4C,E). RT-qPCR confirmed the RNAseq results as at the age of 2-, 6- and 8 months, the males showed decreased expression of Cyp2c29 (FC = −2.3, 5.0 and 5.6, with $p \leq .001$, $p = .003$ and $p = .01$, respectively) and Cyp2c50 (FC = −3.79, −9.9, and 7.8, with $p \leq .001$, $p = .021$ and, $p = .002$, respectively). Both these pathways analyzed are alternative downstream metabolic pathways of AA (Figure 4F). In addition, many genes involved in AA metabolism were up or downregulated in the LiB12cKO

TABLE 2 Serum liver profile results.

	Males				Females			
Parameter	**CTRL ($n = 8$)**	**KO ($n = 10$)**	**FC**	***p*-value**	**CTRL ($n = 10$)**	**KO ($n = 10$)**	**FC**	***p*-value**
Alkaline phosphatase (U/L)	100 ± 21.1	602 ± 238	6.00	<.001***	160 ± 18.8	411 ± 117	2.57	<.001***
Alanine aminotransferase (U/L)	60.3 ± 47.3	486 ± 143	8.06	<.001***	26.0 ± 4.64	168 ± 48.1	6.45	<.001***
Gamma-glutamyl transferase (U/L)	5.00 ± 0.00	5.40 ± 0.97	1.08	.477ns	5.00 ± 0.00	5.00 ± 0.00	1.00	>.999ns
Bile acids (umol/L)	3.57 ± 6.80	18.0 ± 24.6	5.04	.020*	18.3 ± 44.1	24.6 ± 41.8	1.34	.028
Total bilirubin (umol/L)	4.00 ± 0.76	4.60 ± 1.27	1.15	.255ns	4.30 ± 0.82	4.40 ± 1075	1.02	.903ns
Albumin (g/L)	35.9 ± 6.01	42.6 ± 2.41	1.19	.005**	43.1 ± 1.52	42.7 ± 1.83	−1.01	.742ns
Blood urea nitrogen (mmol/L)	6.80 ± 2.02	7.80 ± 1.45	1.15	.238ns	6.27 ± 1.24	6.96 ± 1.75	1.11	.323ns
Total cholesterol (mmol/L)	3.15 ± 0.42	3.50 ± 0.77	1.11	.268ns	2.96 ± 0.35	2.24 ± 0.40	−1.32	<.001***

Abbreviations: CTRL, control; FC, fold change; KO, knockout.

ns = not significant, *p < 0.05, **p < 0.01, ***p < 0.001.

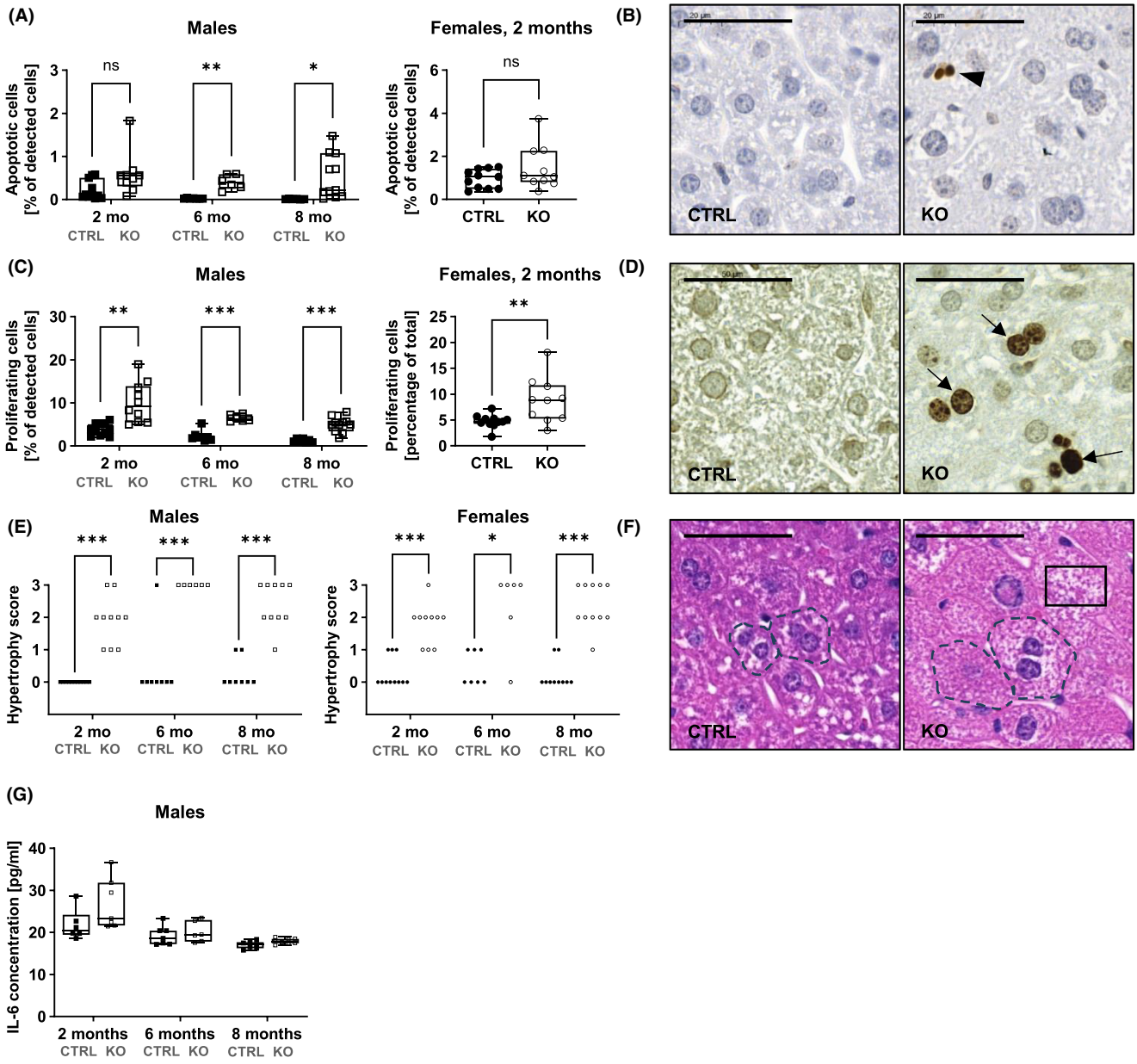

FIGURE 3 Histological images of LiB12cKO (KO) liver tissue. (A) Quantification of apoptotic cells by TUNEL staining and image analysis, (B) representative image of an apoptotic cell (arrowhead). (C) Quantification of proliferative cells by Ki-67 staining and image analysis. (D) Representative image of proliferative cells (black arrows). (E) Hypertrophy score in male and female mice (F) and representative image of hypertrophic cells. Dotted lines indicate cell borders. An example of a rarified cytoplasm can be seen inside the rectangle. (G) Serum concentrations of IL-6 in male mice. Scale bars = 50 μm. ns = not significant, *$p < 0.05$, **$p < 0.01$, ***$p < 0.001$.

mice. However, in the enrichment analysis of the differentially expressed genes no inflammation-related term was found in the top 20 summary terms (Table S1).

4 | DISCUSSION

We have previously shown that disrupting the *Hsd17b12* gene is essential for early fetal development in mice,[8] with the defect in the cell proliferation as early as at the blastocyst stage. This indicates a key role for the enzyme in cell survival at an early stage of embryonic development. Furthermore, disrupting HSD17B12 function globally in adult mice with the inducible *Cre-loxP* technique leads to a rapid loss of almost all the adipose tissue and general indisposition, accompanied by liver damage within 6 days after gene deletion.[10] In line with this phenotype, HSD17B12 has been identified as a gene associated with body adiposity in many human genome-wide association study databases, such as UK Biobank (https://www.ukbiobank.ac.uk/), as well as in reports with humans and cattle.[21–24] Others have also shown that together with the

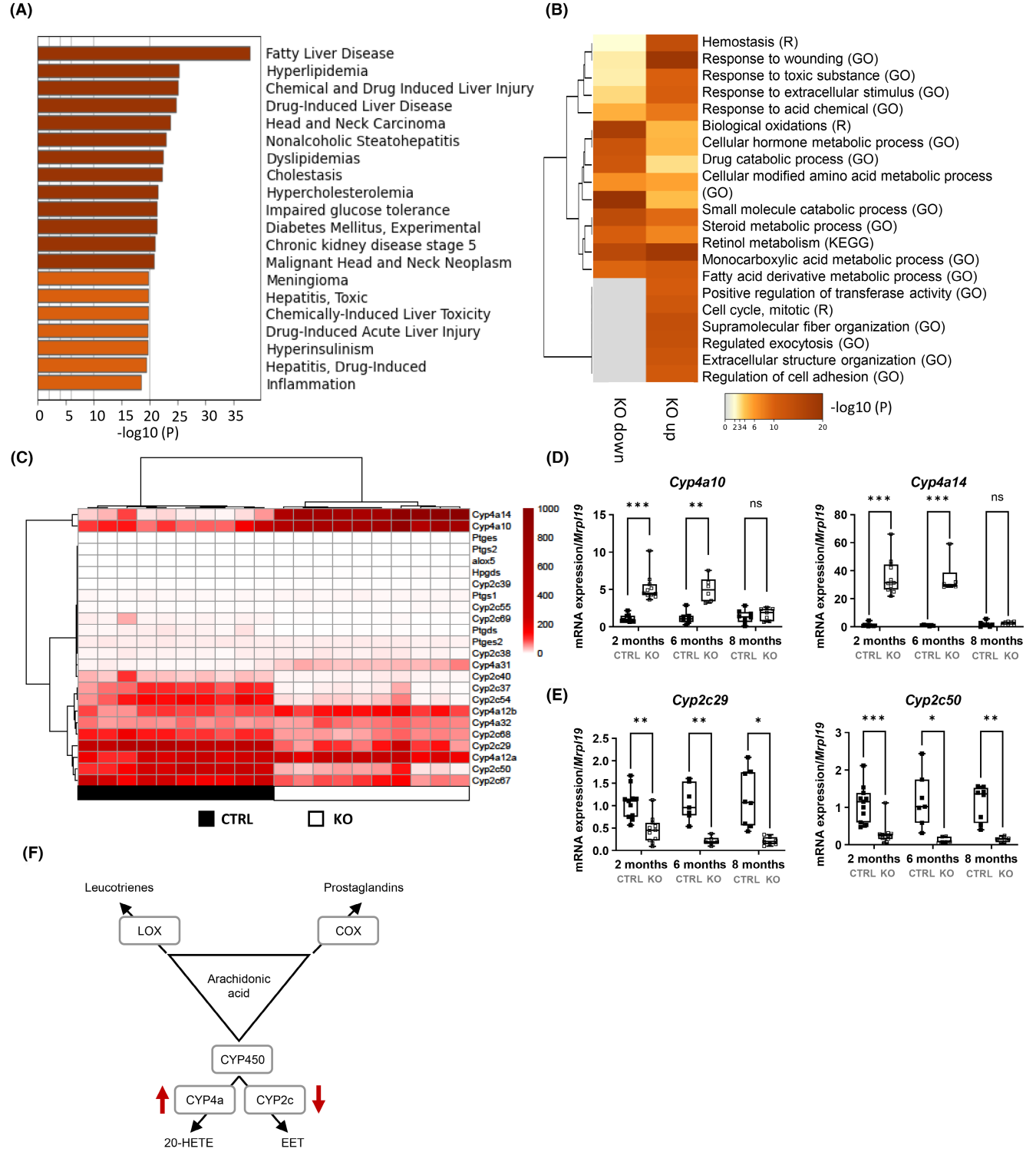

FIGURE 4 Transcriptomic analysis of the liver in LiB12cKO males at the age of 2 months. Functional enrichment analysis of differentially regulated genes (false discovery rate <0.05, fold change (FC) >2, >1 reads per kilobase per million mapped reads (RPKM) of LiB12cKO (KO) (n = 10) vs. control (CTRL) (*n* = 10) livers with (A) DisGeNET Gene Disease Database and (B) Metascape pathway databases. For (A) up and downregulated genes were analyzed together and for (B) separately. Analysis was conducted at metascape.org and included functional categories from Gene Ontology Biological Processes (GO), KEGG (K), and Reactome (R). (C) mRNA expression of genes involved in arachidonic acid metabolism, RPKM. (D) The expression of cytochrome P450 4a10 (*Cyp4a10*) and *Cyp4a14* as well as (E) *Cyp2c29* and *Cyp2c50* in 2-, 6-, and 8-month-old male mice by RT-qPCR. (F) A chart illustrating metabolites synthesized from arachidonic acid. ns = not significant, *p < 0.05, **p < 0.01, ***p < 0.001.

size of body fat, the enzyme controls fat cell number, and diabetes risk in experimental models.[25] However, our data obtained after deleting the enzyme in vivo with the *Cre-lox* recombination in mature adipocytes in mice showed no difference in the number or size of the adipocytes between the KO and WT adipocytes.[10] This suggests that the enzyme more likely has a role in adipocyte differentiation than in the function of the mature adipocytes.

Expression of *Hsd17b12* is high in the liver in both humans and mice,[10,26] and the liver is an important organ in body weight regulation and energy metabolism. In the present study, we thus have created a hepatocyte-specific *Hsd17b12* KO mouse strain. The study revealed that the absence of HSD17B12 activity in the hepatocytes from the fetal period onward does not replicate the dramatic, and rapid, weight loss and lethal phenotype observed in the inducible global KO, and no difference was observed in the body weight between CTRL s and LiB12cKO mice at the age of 2 months. However, lower body weight in the LiB12cKO mice compared with CTRL s was evident at the age of 6 months (females) and 8 months in both sexes. The cause and significance of the small decrease in the lean mass measured in 6-month-old male LiB12cKO mice, normalized at 8 months of age, is not known, and could be associated with the overall reduced body weight. This demonstrates the role of the hepatocyte-expressed HSD17B12 in the regulation of whole-body adiposity. However, the reduction in body weight was much milder than that observed in the whole-body KO induced at adult age, where the disruption of *Hsd17b12* affects most tissues, while in the LiB12cKO-mice the gene disruption is limited to the liver. Therefore, in the Rosa26CreERT model, the effects on the liver also come from several tissues and may be accumulative. In line with the data from others showing an association of HSD17B12 with diabetic risk,[25,27,28] the present data in LiB12cKO mice indicated that LiB12cKO male mice present with increased glucose tolerance. These data together show that the phenotype of the LiB12cKO mice is not associated with increased body adiposity and insulin resistance and therefore does not mimic the type of NAFLD that is increasing in prevalence in Western countries, rather it mimics the fatty liver disease occurring in lean individuals.

In analyses in vitro, HSD17B12 has been shown to be involved in the very long-chain FA (VLCFA) synthesis.[7] Our data show that HSD17B12 deficiency does not fully block FA elongation and the production of the VLCFAs in mouse hepatocytes in vivo. The main support for the hypothesis that HSD17B12 is involved in FA elongation comes from a study by Moon and Horton, who in 2003 performed in vitro fatty assays using palmitic (16:0), γ-linolenic (18:3n-6), arachidonic (20:4n-6), and eicosapentaenoic acid (20:5n-3) as substrates and observed an accumulation of 3-ketoacyl-CoA intermediates.[7] This misalignment of in vivo data with the in vitro results may be due to the compensatory enzymatic activity in a living organism, as there are more substrates available and various processes affecting cellular metabolism. On the other hand, our data does not exclude the possibility of HSD17B12 involvement in FA elongation, as the possible compensatory activity could mask the effects of HSD17B12 disruption. HSD17B12 knock-down in cells has been shown to reduce the number and size of LDs.[29] This is in line with our present data suggesting a defect in the LD biogenesis and LD expansion in the LiB12cKO mice. Despite markedly increased fat accumulation (10-fold for CEs and more than fourfold for triglycerides) the livers of the LiB12cKO mice showed mostly small LDs. This caused increasing areas of microvesicular steatosis, while macrovesicular steatosis did not increase. However, our lipidomics data revealed a reduced amount of certain lipid species, especially PC and PE, with FAs with carbon chain lengths of 18 and 20 atoms, including oleic acid. These lipids have been shown to act in the process of LD coalescence,[30,31] further supporting our assumption that hepatocytes in the LiB12cKO mice present with a misbalance in the LD expansion.

Similarly, others have recently shown that depletion of HSD17B12 in vitro results in a drastic reduction of LD size.[29] In the same study, HSD17B12 deficiency was also shown to impair virus replication, presumably due to a defect in the production of the membrane-coated virus particles. LD formation also protects the tissue from lipotoxicity,[32] and dysfunction of the LD formation may be one of the reasons for the signs of toxicity observed in LiB12cKO livers, observed as an increased number of hepatocytes undergoing apoptotic cell death and increased ALT and ALP in the serum, in the presence of only mild steatosis. Surprisingly, SM concentration, a component of the LD membrane, was reduced in the KO liver. However, the relevance of this finding is not clear, as previous studies indicate that its concentration in LDs is relatively low.[33,34]

Due to the observed role of HSD17B12 in FA elongation, the enzyme has also proposed to be a key player in the production of arachidonic acid (AA)[7] and its downstream eicosanoid metabolites.[9] Our present lipidomic analysis results do not directly support a vital role in AA production in vivo, as the AA levels were not reduced in the LiB12cKO livers several weeks after the gene disruption. However, we found a change in the expression of several genes involved in the synthesis of prostaglandins and AA metabolism. Most notably, we observed an increased expression of the *Cyp4a* family of genes, which are involved in the synthesis of 20-HETE, a compound with vasoconstrictor properties.[35] In contrast,

several Cyp2c epoxygenases were downregulated in the LiB12KO livers. These enzymes metabolize AA to EET, a biologically active compound with anti-inflammatory and vasodilatory properties.[36,37] These findings suggest that the disruption of *Hsd17b12* in the liver shifts the AA consumption from epoxidation toward omega-hydroxylation (from EET toward 20-HETE). This change could also partly explain the liver phenotype in the LiB12KO mice, as data exist linking decreased serum EET concentration and NAFLD in humans, and it has been shown that reduced CYP epoxygenase activity worsens the NASH phenotype.[38] 20-HETE has been shown to possess mitogenic properties,[39] which could explain the increased hepatocyte proliferation.

Similar to HSD17B12, the cell death-inducing DFF45-like effector C (Cidec) is an LD and endoplasmic reticulum-associated protein, known to promote TAG storage and LD formation in adipocytes.[40–42] Furthermore, depending on the isoform, CIDEC determines the development of either one large LD (white fat) or several small LDs (brown fat).[43] The increased expression of *CIDEC* mRNA observed by RNaseq in the LiB12cKO livers could be a response to the dysfunction in the LD expansion and microvesicular steatosis. Other interesting findings include the increased expression of *Flot1*. This LD-associated protein has been shown to facilitate the interactions between LDs and endoplasmic reticulum.[44–46] The RNAseq data of LiB12cKO livers also indicated a downregulation of several members of the major urinary protein gene family. Those proteins are highly expressed exclusively in males and are known to mediate sexual signature in mice as male-specific pheromones.[47] Interestingly, recent data have suggested that especially major urinary protein 1 is a specific marker for endoplasmic reticulum stress,[48] well in line with the localization of HSD17B12 in the endoplasmic reticulum and the deficiency in the endoplasmic reticulum-related LD expansion. Furthermore, the liver phenotype in LiB12cKO males was more pronounced compared with female mice. This and data from other animal models of NAFLD are in line with the data from humans pointing toward a sex difference in the susceptibility to NAFLD. In humans, men and postmenopausal women are at higher risk of developing fatty liver disease compared with premenopausal women.[49] Estrogens seem to protect against NAFLD, as postmenopausal women are affected twice as often as premenopausal.[50] In addition, sex steroids are known to regulate the immune system and therefore affect hepatic inflammation.[51] Male and female livers have also been shown to differ in their susceptibility to toxicity.[52]

In conclusion, hepatocyte-specific *Hsd17b12* disruption results in a complex outcome with increased microvesicular steatosis and liver damage. We have shown that the initial phenotype is related to the dysfunction in the LD formation/expansion, resulting in an excess lipid load in the liver also causes lipotoxicity in the tissue. There is evidence that storing excess lipids in a neutral form in the LD minimizes the potentially toxic effects of TAG accumulation and serves as a defense against lipotoxicity.[53] The transcriptomic analysis revealed that the expression changes matched widely with those observed in fatty liver disease in humans, suggesting that this KO mouse model mimics NAFLD in non-obese individuals.

AUTHOR CONTRIBUTIONS

H.H., L.M., S.T.R., L.S., and M.P. conceived and designed the research; H.H., S.T.R., and L.M. performed experiments; H.H., L.M., K.T.R., S.D.B., A.L., S.K., T.S., analyzed the data; H.H., L.M., S.T.R., K.T.R., S.D.B., L.L.E., L.S., and M.P. interpreted the results of the experiments; H.H., L.M., K.T.R., A.L., S.K., and T.S., prepared the figures; H.H. drafted the manuscript; H.H, L.M., K.T.R., L.S., and M.P. edited and revised the manuscript; H.H., L.M., S.T.R., K.T.R., S.D.B., A.L., S.K., T.S., L.L.E., L.S., and M.P. approved the final version of manuscript.

ACKNOWLEDGMENTS

The authors thank the whole personnel of the Turku Center for Disease Modeling, especially Madeleine Latvala, Nina Messner, Heli Niittymäki, Katri Hovirinta, Jonna Palmu, Mona Niiranen and Clara-Theresia Kolehmainen, the Histology Core Facility at the Institute of Biomedicine, University of Turku, and the Central Animal Laboratory at the University of Turku, as well as the personnel of the Metabolomics Unit, Technology Center, Institute for Molecular Medicine, University of Helsinki, Finland. Turku Center for Disease Modeling is part of the Biocenter Finland Model Organisms Infrastructure. Our research was also supported by the Biocenter Finland Bioinformatics platform and ELIXIR Finland.

FUNDING INFORMATION

This work was funded by the Sigrid Jusélius Foundation, Jalmari and Rauha Ahokas Foundation, the Drug Research Doctoral Programme at the University of Turku, and the University of Turku.

DISCLOSURES

The authors declare no conflict of interest.

DATA AVAILABILITY STATEMENT

The RNAseq data that support the findings of this study are openly available at Gene Expression Omnibus (RRID:SCR_005012) repository under the series accession number GSE255345.

ORCID

Hanna Heikelä https://orcid.org/0000-0002-3971-6992
Laura Mairinoja https://orcid.org/0000-0003-3552-5416
Suvi T. Ruohonen https://orcid.org/0000-0001-9141-7052
Kalle T. Rytkönen https://orcid.org/0000-0002-5138-0889
Simone de Brot https://orcid.org/0000-0003-3049-0103
Asta Laiho https://orcid.org/0000-0001-6217-6659
Satu Koskinen https://orcid.org/0000-0003-0149-2070
Tomi Suomi https://orcid.org/0000-0003-3639-979X
Laura L. Elo https://orcid.org/0000-0001-5648-4532
Leena Strauss https://orcid.org/0000-0002-5682-205X
Matti Poutanen https://orcid.org/0000-0002-8953-1734

REFERENCES

1. Younossi ZM, Golabi P, Paik JM, Henry A, Van Dongen C, Henry L. The global epidemiology of nonalcoholic fatty liver disease (NAFLD) and nonalcoholic steatohepatitis (NASH): a systematic review. *Hepatology*. 2023;77(4):1335-1347. doi:10.1097/hep.0000000000000004
2. Smith GI, Shankaran M, Yoshino M, et al. Insulin resistance drives hepatic de novo lipogenesis in nonalcoholic fatty liver disease. *J Clin Invest*. 2020;130(3):1453-1460. doi:10.1172/JCI134165
3. Singh S, Allen AM, Wang Z, Prokop LJ, Murad MH, Loomba R. Fibrosis progression in nonalcoholic fatty liver vs nonalcoholic steatohepatitis: a systematic review and meta-analysis of paired-biopsy studies. *Clin Gastroenterol Hepatol*. 2015;13(4):643-654. e9. doi:10.1016/j.cgh.2014.04.014
4. Targher G, Byrne CD, Tilg H. NAFLD and increased risk of cardiovascular disease: clinical associations, pathophysiological mechanisms and pharmacological implications. *Gut*. 2020;69(9):1691-1705. doi:10.1136/gutjnl-2020-320622
5. Dufort I, Rheault P, Huang XF, Soucy P, Luu-The V. Characteristics of a highly labile human type 5 17-hydroxysteroid dehydrogenase. *Endocrinology*. 1999;140(2):568-574. https://academic.oup.com/endo/article/140/2/568/2990286
6. Mindnich R, Möller G, Adamski J. The role of 17 beta-hydroxysteroid dehydrogenases. *Mol Cell Endocrinol*. 2004;218:7-20. doi:10.1016/j.mce.2003.12.006
7. Moon YA, Horton JD. Identification of two mammalian reductases involved in the two-carbon fatty acyl elongation cascade. *J Biol Chem*. 2003;278(9):7335-7343. doi:10.1074/jbc.M211684200
8. Rantakari P, Lagerbohm H, Kaimainen M, et al. Hydroxysteroid (17β) dehydrogenase 12 is essential for mouse organogenesis and embryonic survival. *Endocrinology*. 2010;151(4):1893-1901. doi:10.1210/en.2009-0929
9. Kemiläinen H, Adam M, Mäki-Jouppila J, et al. The hydroxysteroid (17β) dehydrogenase family gene HSD17B12 is involved in the prostaglandin synthesis pathway, the ovarian function, and regulation of fertility. *Endocrinology*. 2016;157(10):3719-3730. doi:10.1210/en.2016-1252
10. Heikelä H, Ruohonen ST, Adam M, et al. Hydroxysteroid (17β) dehydrogenase 12 is essential for metabolic homeostasis in adult mice. *Am J Physiol Endocrinol Metab*. 2020;319(3):E494-E508. doi:10.1152/ajpendo.00042.2020
11. Postic C, Shiota M, Niswender KD, et al. Dual roles for glucokinase in glucose homeostasis as determined by liver and pancreatic cell-specific Gene Knock-outs using Cre recombinase. *J Biol Chem*. 1999;274(1):305-315. doi:10.1074/jbc.274.1.305
12. Mukarami T, Yasuda Y, Mita S, et al. Prealbumin gene expression during mouse development studied by in situ hybridization. *Cell Differ Dev*. 1987;22(1):1-9. doi:10.1016/0045-6039(87)90408-8
13. Weisend CM, Kundert JA, Suvorova ES, Prigge JR, Schmidt EE. Cre activity in fetal albCre mouse hepatocytes: utility for developmental studies. *Genesis*. 2009;47(12):789-792. doi:10.1002/dvg.20568
14. Postic C, Magnuson MA. DNA excision in liver by an albumin-Cre transgene occurs progressively with age. *Genesis*. 2000;26(2):149-150. doi:10.1002/(sici)1526-968x(200002)26:2<149::aid-gene16>3.0.co;2-v
15. Mairinoja L, Heikelä H, Blom S, et al. Deep learning based image analysis of liver steatosis in mouse models. *Am J Pathol*. 2023;193(8):1072-1080. doi:10.1016/j.ajpath.2023.04.014
16. Bankhead P, Loughrey MB, Fernández JA, et al. QuPath: open source software for digital pathology image analysis. *Sci Rep*. 2017;7(1):16878. doi:10.1038/s41598-017-17204-5
17. Andrews S. *FastQC: A Quality Control Tool for High Throughput Sequence Data*. The Babraham Institute. 2019. Accessed July 18, 2022. http://www.bioinformatics.babraham.ac.uk/projects/fastqc
18. Liao Y, Smyth GK, Shi W. The R package Rsubread is easier, faster, cheaper and better for alignment and quantification of RNA sequencing reads. *Nucleic Acids Res*. 2019;47(8):e47. doi:10.1093/nar/gkz114
19. Robinson MD, Mccarthy DJ, Smyth GK. edgeR: a Bioconductor package for differential expression analysis of digital gene expression data. *Bioinformatics*. 2010;26(1):139-140. doi:10.1093/bioinformatics/btp616
20. Suomi T, Seyednasrollah F, Jaakkola MK, Faux T, Elo LL. ROTS: an R package for reproducibility-optimized statistical testing. *PLoS Comput Biol*. 2017;13(5):e1005562. doi:10.1371/journal.pcbi.1005562
21. Hachim MY, Aljaibeji H, Hamoudi RA, et al. An integrative phenotype–genotype approach using phenotypic characteristics from the UAE national diabetes study identifies HSD17B12 as a candidate gene for obesity and type 2 diabetes. *Genes (Basel)*. 2020;11(4):461. doi:10.3390/genes11040461
22. Carless MA, Kulkarni H, Kos MZ, et al. Genetic effects on DNA methylation and its potential relevance for obesity in Mexican Americans. *PLoS One*. 2013;8(9):e73950. doi:10.1371/journal.pone.0073950
23. Liu J, Che Y, Cai K, et al. miR-136 regulates the proliferation and Adipogenic differentiation of adipose-derived stromal vascular fractions by targeting HSD17B12. *Int J Mol Sci*. 2023;24(19):14892. doi:10.3390/ijms241914892
24. Du L, Li K, Chang T, et al. Integrating genomics and transcriptomics to identify candidate genes for subcutaneous fat deposition in beef cattle. *Genomics*. 2022;114(4):110406. doi:10.1016/j.ygeno.2022.110406
25. Kulyte A, Aman A, Strawbridge RJ, Arner P, Dahlman IA. Genome-wide association study identifies genetic loci associated with fat cell number and overlap with genetic risk loci for type 2 diabetes. *Diabetes*. 2022;71(6):1350-1362. doi:10.2337/db21-0804
26. Sakurai N, Miki Y, Suzuki T, et al. Systemic distribution and tissue localizations of human 17beta-hydroxysteroid dehydrogenase type 12. *J Steroid Biochem Mol Biol*. 2006;99(4–5):174-181. doi:10.1016/j.jsbmb.2006.01.010

27. Giordo R, Gulsha R, Kalla S, Calin GA, Lipovich L. LncRNA-associated genetic etiologies are shared between type 2 diabetes and cancers in the UAE population. *Cancers (Basel)*. 2022;14(14):3313. doi:10.3390/cancers14143313
28. Scott RA, Scott LJ, Mägi R, et al. An expanded genome-wide association study of type 2 diabetes in Europeans. *Diabetes*. 2017;66(11):2888-2902. doi:10.2337/db16-1253
29. Mohamed B, Mazeaud C, Baril M, et al. Very-long-chain fatty acid metabolic capacity of 17-beta-hydroxysteroid dehydrogenase type 12 (HSD17B12) promotes replication of hepatitis C virus and related flaviviruses. *Sci Rep*. 2020;10(1):4040. doi:10.1038/s41598-020-61051-w
30. Krahmer N, Guo Y, Wilfling F, et al. Phosphatidylcholine synthesis for lipid droplet expansion is mediated by localized activation of CTP:Phosphocholine cytidylyltransferase. *Cell Metab*. 2011;14(4):504-515. doi:10.1016/j.cmet.2011.07.013
31. Guo Y, Walther TC, Rao M, et al. Functional genomic screen reveals genes involved in lipid-droplet formation and utilization. *Nature*. 2008;453(7195):657-661. www.nature.com/nature
32. Zadoorian A, Du X, Yang H. Lipid droplet biogenesis and functions in health and disease. *Nat Rev Endocrinol*. 2023;19(8):443-459. doi:10.1038/s41574-023-00845-0
33. Chitraju C, Trötzmüller M, Hartler J, et al. Lipidomic analysis of lipid droplets from murine hepatocytes reveals distinct signatures for nutritional stress. *J Lipid Res*. 2012;53(10):2141-2152. doi:10.1194/jlr.M028902
34. Bartz R, Li WH, Venables B, et al. Lipidomics reveals that adiposomes store ether lipids and mediate phospholipid traffic. *J Lipid Res*. 2007;48:837-847. doi:10.1194/jlr.M600413-JLR200
35. Imig JD. Epoxyeicosatrienoic acids, 20-hydroxyeicosatetraenoic acid, and renal microvascular function. *Prostaglandins Other Lipid Mediat*. 2013;104-105:2-7. doi:10.1016/j.prostaglandins.2013.01.002
36. Zhang Y, Oltman CL, Lu T, Lee HC, Dellsperger KC, Vanrollins M. EET homologs potently dilate coronary microvessels and activate BKCa channels. *Am J Physiol Heart Circ Physiol*. 2001;280:2430-2440. doi:10.1152/ajpheart.2001.280.6.H2430
37. Node K, Huo Y, Ruan X, et al. Anti-inflammatory properties of cytochrome P450 epoxygenase-derived eicosanoids. *Science*. 1999;285(5431):1276-1279.
38. Arvind A, Osganian SA, Sjoquist JA, Corey KE, Simon TG. Epoxygenase-derived Epoxyeicosatrienoic acid mediators are associated with nonalcoholic fatty liver disease, nonalcoholic steatohepatitis, and fibrosis. *Gastroenterology*. 2020;159(6):2232-2234.e4. doi:10.1053/j.gastro.2020.08.001
39. Lin F, Rios A, Falck JR, Belosludtsev Y, Schwartzman ML. 20-Hydroxyeicosatetraenoic acid is formed in response to EGF and is a mitogen in rat proximal tubule. *Am J Phys*. 1995;269(6):F806-F816. doi:10.1152/ajprenal.1995.269.6.F806
40. Puri V, Konda S, Ranjit S, et al. Fat-specific protein 27, a novel lipid droplet protein that enhances triglyceride storage. *J Biol Chem*. 2007;282(47):34213-34218. doi:10.1074/jbc.M707404200
41. Nian Z, Sun Z, Yu L, Toh SY, Sang J, Li P. Fat-specific protein 27 undergoes ubiquitin-dependent degradation regulated by triacylglycerol synthesis and lipid droplet formation. *J Biol Chem*. 2010;285(13):9604-9615. doi:10.1074/jbc.M109.043786
42. Lyu X, Wang J, Wang J, et al. A gel-like condensation of Cidec generates lipid-permeable plates for lipid droplet fusion. *Dev Cell*. 2021;56(18):2592-2606.e7. doi:10.1016/j.devcel.2021.08.015
43. Nishimoto Y, Tamori Y. CIDE family-mediated unique lipid droplet morphology in white adipose tissue and brown adipose tissue determines the adipocyte energy metabolism. *J Atheroscler Thromb*. 2017;24(10):989-998. doi:10.5551/jat.RV17011
44. Liu P, Ying Y, Zhao Y, Mundy DI, Zhu M, Anderson RGW. Chinese hamster ovary K2 cell lipid droplets appear to be metabolic organelles involved in membrane traffic. *J Biol Chem*. 2004;279(5):3787-3792. doi:10.1074/jbc.M311945200
45. Rajendran L, Le Lay S, Illges H. Raft association and lipid droplet targeting of flotillins are independent of caveolin. *Biol Chem*. 2007;388(3):307-314. doi:10.1515/BC.2007.034
46. Sadh K, Rai P, Mallik R. Feeding-fasting dependent recruitment of membrane microdomain proteins to lipid droplets purified from the liver. *PLoS One*. 2017;12(8):e0183022. doi:10.1371/journal.pone.0183022
47. Hastie ND, Held WA, Toole JJ. Multiple genes coding for the androgen-regulated major urinary proteins of the mouse. *Cell*. 1979;17(2):449-457. doi:10.1016/0092-8674(79)90171-5
48. Gao R, Wang H, Li T, et al. Secreted MUP1 that reduced under ER stress attenuates ER stress induced insulin resistance through suppressing protein synthesis in hepatocytes. *Pharmacol Res*. 2023;187:187. doi:10.1016/j.phrs.2022.106585
49. Lonardo A, Nascimbeni F, Ballestri S, et al. Sex differences in nonalcoholic fatty liver disease: state of the art and identification of research gaps. *Hepatology*. 2019;70(4):1457-1469. doi:10.1002/hep.30626
50. Hamaguchi M, Kojima T, Ohbora A, Takeda N, Fukui M, Kato T. Aging is a risk factor of nonalcoholic fatty liver disease in premenopausal women. *World J Gastroenterol*. 2012;18(3):237-243. doi:10.3748/wjg.v18.i3.237
51. Della Torre S. Non-alcoholic fatty liver disease as a canonical example of metabolic inflammatory-based liver disease showing a sex-specific prevalence: relevance of estrogen signaling. *Front Endocrinol (Lausanne)*. 2020;11:572490. doi:10.3389/fendo.2020.572490
52. Wahlang B, Hardesty JE, Head KZ, et al. Hepatic injury caused by the environmental toxicant vinyl chloride is sex-dependent in mice. *Toxicol Sci*. 2020;174(1):79-91. doi:10.1093/toxsci/kfz236
53. Listenberger LL, Han X, Lewis SE, et al. Triglyceride accumulation protects against fatty acid-induced lipotoxicity. *PNAS*. 2003;100(6):3077-3082. www.pnas.orgcgidoi10.1073pnas.0630588100

SUPPORTING INFORMATION

Additional supporting information can be found online in the Supporting Information section at the end of this article.

How to cite this article: Heikelä H, Mairinoja L, Ruohonen ST, et al. Disruption of HSD17B12 in mouse hepatocytes leads to reduced body weight and defect in the lipid droplet expansion associated with microvesicular steatosis. *The FASEB Journal*. 2024;38:e70034. doi:10.1096/fj.202400333RR